ORIGINAL PAPER

CrossMark

Morphology Conserving High Efficiency Nitrogen Doping of Titanate Nanotubes by NH$_3$ Plasma

Balázs Buchholcz[1] · Kamilla Plank[1] · Miklós Mohai[2] · Ákos Kukovecz[1] · János Kiss[3,4] · Imre Bertóti[2] · Zoltán Kónya[1,4]

Abstract

Titanate nanotubes offer certain benefits like high specific surface area, anisotropic mesoporous structure and ease of synthesis over other nanostructured titania forms. However, their application in visible light driven photocatalysis is hindered by their wide band-gap, which can be remedied by, e.g., anionic doping. Here we report on a systematic study to insert nitrogen into lattice positions in titanate nanotubes. The efficiency of N$_2^+$ bombardment, N$_2$ plasma and NH$_3$ plasma treatment is compared to that of NH$_3$ gas synthesized *in situ* by the thermal decomposition of urea or NH$_4$F. N$_2^+$ bombarded single crystalline rutile TiO$_2$ was used as a doping benchmark (16 at.% N incorporated). Surface species were identified by diffuse reflectance infrared spectroscopy, structural features were characterized by scanning electron microscopy and powder X-ray diffraction measurements. The local chemical environment of nitrogen built into the nanotube samples was probed by X-ray photoelectron spectroscopy. Positively charged NH$_3$ plasma treatment offered the best doping performance. This process succeeded in inserting 20 at.% N into nanotube lattice positions by replacing oxygen and forming Ti–N bonds. Remarkably, the nanotubular morphology and titanate crystal structure were both fully conserved during the process. Since plasma treatment is a readily scalable technology, the suggested method could be utilized in developing efficient visible light driven photocatalysts based on N-doped titanate nanotubes.

Keywords Titanate nanotube · N-doping · NH$_3$ plasma · Morphology · Anatase

✉ Balázs Buchholcz
  buchholcz@chem.u-szeged.hu

✉ Zoltán Kónya
  konya@chem.u-szeged.hu

1   Department of Applied and Environmental Chemistry, University of Szeged, Rerrich B. 1, Szeged 6720, Hungary

2   Hungarian Academy of Sciences (HAS), Research Centre of Natural Sciences, Institute of Materials and Environmental Chemistry, Magyar tudósok körútja 2, Budapest 1117, Hungary

3   Department of Physical Chemistry and Materials Science, University of Szeged, Aradi vértanúk tere 1, Szeged 6720, Hungary

4   MTA-SZTE Reaction Kinetics and Surface Chemistry Research Group, University of Szeged, Rerrich B. 1, Szeged 6720, Hungary

1 Introduction

Layered titanate nanotubes (TiONT) have attracted considerable attention in the past two decades because of their relatively high specific surface area and pore volume, interesting open-ended tubular morphology [1, 2] and ability to stabilize metal nanoparticles [3, 4], metal oxides [5] or multicomponent semiconductors on their surface [6]. These properties render TiONTs a potential catalyst or catalyst support in thermal [7, 8] and photo-activated chemical reactions [9–11]. Moreover, titanate nanotubes can be used as ion-exchangers [12], adsorbents [13] or in different biomedical applications [14, 15]. The chemical formula of TiONTs can be described as Na$_2$Ti$_3$O$_7$ or H$_2$Ti$_3$O$_7$, the latter being the protonated form of the as-synthesized former structure. Peng et al. offered a mixed cationic formula: Na$_x$H$_{2-x}$Ti$_3$O$_7$ [16] that is probably the most appropriate for referring to a general TiONT sample.

TiONTs can be synthesized from a broad variety of titanium-oxides made up of TiO$_6$ octahedra, e.g. anatase, rutile, brookite and certain salts of titanic acid [17, 18].

At the first glance, TiONTs seem to be very different from titanium-dioxides, but actually, there are many similarities in the properties of this titanium-oxide based material and TiO$_2$ [16]. Finding these similarities and differences between TiO$_2$ and TiONT is a key direction in contemporary titania nanostructure research [5].

TiO$_2$ is among the most popular metal-oxide semiconductors in the field of UV-light driven photocatalysis [19–22]. Its ability to generate electron–hole pairs by incident light with appropriate wavelength and use them in redox reactions makes TiO$_2$ a favorable "green-chemical" catalyst [23]. The anatase and rutile forms of TiO$_2$ have relative large indirect band-gap (E$_g$) with 3.2 and 3.0 eV, respectively. Electron mobility is higher in anatase than in rutile. Unfortunately, TiO$_2$ absorbs only 6% of solar light in the UV-range, whereas 50% of the energy arriving to the Earth at sea level is between 400 and 700 nm. Many research groups work on developing TiO$_2$-based photocatalysts that are excitable by the lower energy part of electromagnetic spectrum, namely the UV–Vis [24], visible [25] and NIR [26, 27] (near infrared) ranges. Today, several methods are available to prepare TiO$_2$ based visible light photocatalysts, but the ultimate high performance material is yet to be discovered.

Doping is a well-known method to decrease the band gap energy or create mid-gap states in the band structure by incorporating foreign atoms into the lattice [28]. Such dopants can be metallic [29, 30] or non-metallic [31, 32], as well as anionic or cationic [33]. For example, the Cr doping of a rutile lattice facilitates its visible light excitation. According to DFT calculations, this is due to TiO$_2$ electrons being excited either from the valence band (VB) into unoccupied Cr mid-gap states or from partially filled Cr mid-gap states into the conduction band by incident visible light. Gracia et al. [34] revealed that even though the Cr, Fe, V and Co doping of anatase results in a red shift of its light absorption spectrum, this process is not necessarily accompanied by the enhancement of the photocatalytic activity. New levels due to dopants can either promote or hinder the recombination of electron–hole pairs. Some dopants can act as recombination centers, whereas doping with e.g. Fe^{3+} or V^{4+} cations brings about longer excited charge carrier lifetimes than those observed in either undoped or Cr, Mn and Co ion modified counterparts [24].

Anionic doping of TiO$_2$ is also an effective way to change its electronic band structure. In 2001, Asahi et al. reported on the nitrogen doping of TiO$_2$ and its enhanced visible light induced photocatalytic activity [35]. The number of publications in this field has increased dramatically since Asahi's pioneering work. Nevertheless, it is worth noting that Sato et al. have published an interesting study about NO$_x$-doped TiO$_2$ and its photocatalytic activity in visible light back in 1986 [36]. Today this paper is generally agreed to be the very first N-doped TiO$_2$ article for

visible light driven (VLD) photocatalysis. Anionic doping by other elements, e.g. B, P, C and S can also tune the optical properties of TiO$_2$ [28]. The general explanation for the effectivity of anionic dopants is that such anions are less electronegative than O, therefore, they push p-states from the VB up into the band-gap when substituted into the lattice. Although these dopants do not affect the thermal stability of TiO$_2$, they can be thermally removed from the system during an annealing process [24]. Unfortunately, the most widespread sol–gel synthesis methods typically involve a final heat-treatment step to achieve well crystallized TiO$_2$ [37].

The thermal stability of titanias depends on their structure. Anatase TiO$_2$ turns into rutile around 600–700 °C [38]. Titanate nanotubes with trititanate structure transform easily into anatase nanorods at ~400 °C, then into rutile at 600 °C. The tubular morphology collapses into a non-layered one between 150 and 200 °C but the one dimensional (1D) structure is preserved. Moreover, TiONT is a metastable material with structural water content [16]. The trititanate to anatase phase transition is thermodynamically favored under ambient conditions, but the transition itself takes at least 1.5–2 years. The thermal stability of titanate nanowires (another 1D titanate nanostructure) is superior to that of TiONTs [39, 40], but their low specific surface area and lack of mesoporous channels make them inappropriate candidates for ionic doping. Titanate nanowires can also stabilize metal nanoparticles on their surface [4].

Nitrogen doping of TiO$_2$ is a well-known approach to create mid-gap states [41]. There are so called wet and dry N doping methods. In the case of wet methods, either the dopant source is mixed with the titania precursor solution or the titania particles are mixed with the solution of the dopant compound. Dry methods generally utilize a gas phase dopant source and solid state titania, e.g. solid TiO$_2$ kept in NH$_3$ gas flow at elevated temperature (400–600 °C) [42]. An example for the wet method is stirring tetra-butyl titanate in the presence of ammonia solution and calcining the dried precursor at 350 °C or higher [43]. Different methods result in different nitrogen sites within the titania structure. X-ray photoelectron spectroscopic (XPS) investigations reveal that there are two (or three) main nitrogen types. The peak at 396 eV binding energy in the N1s region corresponds to the substitutional state mentioned above, where N substitutes O in the lattice. Some articles suggest that this is the type of nitrogen responsible for the improved visible light photocatalytic properties of doped TiO$_2$ [24, 30]. The other main N site has its XPS signal around ~400 eV. This is the so-called interstitial or embedded N that can also decrease the excitation wavelength. In this case reduced Ti^{3+} sites stabilized by the N^{2-} or N^{3-} dopants are formed [44]. It should be noted here that adsorbed N-containing specimens also give rise to an XPS peak around 400 eV.

In our previous study we prepared various nitrogen doped titanium-oxide nanoparticles from protonated titanate nanotubes. The dopant source was NH_3 gas generated in situ by the thermal decomposition of urea in a closed autoclave in the presence of TiONTs at 200 °C [45]. The structure and morphology of doped TiONTs changed with the reaction time. After 12 h the tubular trititanates were transformed into nitrogen-doped anatase nanoparticles. A similar collapse was observed by Chang et al. in the case of NH_4^+ ion exchanged TiONT at elevated temperature [46]. Surface NH_4^+ groups also form during the phase transition. The XPS peak at 396 eV corresponding to Ti–N sites is missing from these spectra, but the ~400 eV signal due to adsorbed NH_x (including NH_3) was observed [41, 47].

Earlier Bertóti investigated N implantation into rutile (110) TiO_2 single crystal and other metal-oxide surfaces via 1–5 keV N_2^+ bombardment [48, 49], which is a highly refined method to investigate nitrogen incorporation into the structure. An oxygen deficient surface formed due to the ion-implantation and metal oxinitride surface developed. The amount of substituted N was equal to that of the reduced oxygen in the lattice [50, 51].

The paramount importance of N-doped TiO_2 in visible light photocatalysis necessitates a paradigm shift in research. Ad hoc doping studies need to be replaced by more systematic efforts. The present study is a step in this direction. We present a comparative investigation on the effects of N_2^+ ion implantation, N_2 and NH_3 plasma treatments on the structure and morphology of titanate nanotubes and on the chemical states of the built-in nitrogen. Results are compared with those obtained by thermal nitridation where the dopants were urea or NH_4F.

2 Experimental

2.1 Synthesis of Titanate Nanotubes

Elongated titanate nanotubes were synthesized by the hydrothermal conversion of TiO_2 (99.8% anatase, Sigma–Aldrich) in highly alkaline media. In a typical process, 50 g TiO_2 precursor was stirred in 1 L 10 M NaOH (99.3% NaOH, Molar) solution for 1 h. The obtained white solid was kept in a polytetrafluoroethylene (PTFE)-lined stainless steel autoclave for 24 h at 130 °C. The reactor was rotated during the synthesis at 3 rpm around its short axis. The product was neutralized by washing with distilled water (2×) and then protonated by washing with 0.01 M HCl solution several times to yield protonated titanate nanotubes ($H_2Ti_3O_7$). Finally, the remaining acid content was washed out from the system with distilled water and the protonated nanotubes were dried at 60 °C for 48 h in air.

2.1.1 Nitrogen Doping

2.1.1.1 Nitrogen Incorporation by N_2^+ Ion Bombardment N_2 and NH_3 Plasma Treatment
Nitrogen was incorporated into titanate nanotubes by N_2^+ bombardment and from N_2 and NH_3 plasma. Ion bombardment was performed within the analysis chamber of the XPS instrument, using a Kratos MacroBeam ion gun fed with high (5N) purity N_2. The ion beam (spot size of about 2 mm, non mass-selected, incident at mean angle 55° to the surface normal) was rastered over the sample area of about 8×8 mm^2. The N_2^+ ions were accelerated by 3 kV, producing N projectiles of 1.5 keV energy. The plasma treatment was performed in the stainless steel sample preparation chamber of the XPS instrument (base pressure $< 1 \times 10^{-4}$ Pa). The high purity N_2 (5N) or NH_3 flow of a few ml/min (STP) was regulated by a bleeding valve that set the pressure to 5–7 Pa. Constant RF power of 100 W at 13.56 MHz was applied through a matching circuit to a copper coil fixed on the outside of a glass dome attached to the preparation chamber. The sample bias was set to negative values between 100 and 300 V. Treatment time was varied from 5 to 30 min. The sample was transferred to the analysis chamber after treatment without exposing it to the ambient air.

2.1.1.2 Thermally Activated Nitrogen Incorporation Method
Two kinds of thermally activated doping processes were applied. Firstly, urea was used as dopant source as reported earlier [45]. In this setup, 12 g urea (99.46%, Molar) and 1 g titanate nanotubes were kept in a PTFE-lined stainless steel autoclave, where the two compounds were separated from each other by a cylindrical PTFE spacer. The system was kept at 200 °C for 24 h. The thermal decomposition of urea yielded the NH_3 gas that acted as the effective nitrogen dopant source.

The second thermal doping method was similar to the previous one. The same system was used to modify the nanotubes, however, 15 g NH_4F was used instead of urea to dope 0.5 g of titanate nanotubes. In this case, thermal decomposition simultaneously yields HF and NH_3 gas that create a potentially more aggressive doping environment.

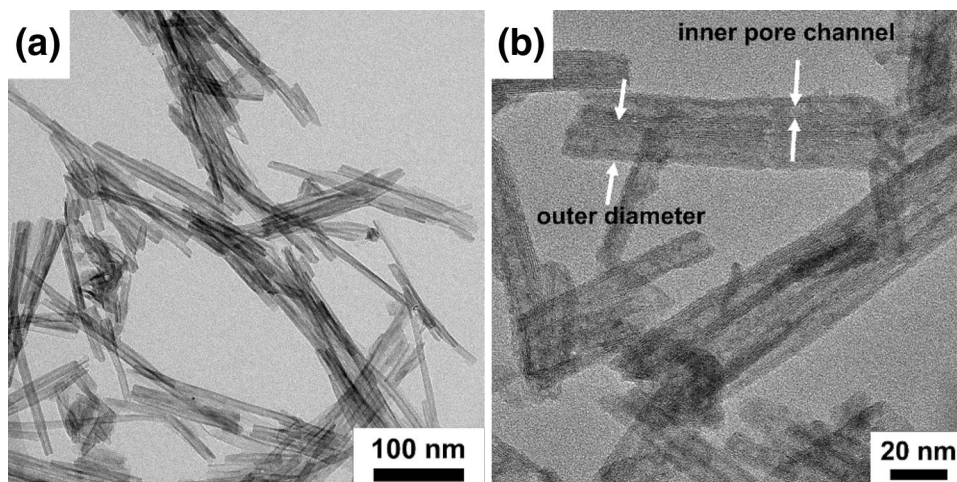### 2.2 Characterization

2.2.1 TEM and SEM Investigation

The morphology of pristine TiONTs and thermally doped nanostructures was analyzed by transmission electron microscopy (TEM) using an FEI Tecnai G^2 20 X-Twin instrument operated at 200 kV accelerating voltage. Samples were drop-casted from their ethanol suspensions onto copper mounted holey carbon grids. The morphological changes of NH_3 plasma modified TiONTs on Al foil were

studied by scanning electron microscopy using a HITACHI S-4700 Type II instrument operated at 30 kV accelerating voltage.

2.2.2 XPS Analysis

X-ray photoelectron spectra of N_2^+ ion bombarded and N_2 and NH_3 plasma treated titanates were recorded on a Kratos XSAM 800 spectrometer operating in fixed analyzer transmission mode, using Mg $K\alpha_{1,2}$ (1253.6 eV) excitation. The pressure in the analysis chamber was lower than 1×10^{-7} Pa. Survey spectra were recorded in the kinetic energy range of 150–1300 eV in 0.5 eV steps. Photoelectron lines of the main constituent elements, i.e. O1s, Ti2p, N1s and C1s, were recorded in 0.1 eV steps and 1 s dwell time. Spectra were referenced to the energy of the C1s line of the carbon contamination, set at 284.6 ± 0.1 eV binding energy (B.E.). A Gaussian–Lorentzian peak shape (70/30 ratio) was used for peak decomposition. Quantitative analysis, based on peak area intensities after removal of the Shirley-type background, was performed by the Kratos Vision 2 and by the XPS MultiQuant programs [52, 53] using the experimentally determined photo-ionization cross-section data of Evans et al. and the asymmetry parameters of Reilman et al. [54]. In all cases, unless otherwise stated, the conventional infinitely thick layer model was employed, where all components are supposed to be homogeneously distributed within the sampling depth detected by XPS. Chemical shifts, representing different bonding states of the nitrogen and oxygen to titanium, were evaluated by applying an accurate peak decomposition procedure. In order to prepare samples for the above treatments, ethanol suspension of TiONT was drop casted onto Al foil to obtain a consistent film-like structure with homogenous nanotube distribution. Films were dried at 100 °C to remove the bulk water from the surface.

2.2.3 XRD Analysis

The crystal structure of TiONTs before and after different nitridation processes was investigated using a Rigaku Miniflex powder X-ray diffractometer with Cu $K\alpha$ irradiation ($\lambda = 1.5418$ Å) operating at 30 kV and 15 mA. The scanning rate was 4°/min in the 5–60° 2θ range.

2.2.4 DRIFTS Measurements

Infrared spectroscopic measurements were carried out in an Agilent Cary-670 FTIR spectrometer equipped with a Harrick Praying Mantis diffuse reflectance attachment. The sample holder had BaF_2 windows in the IR light path. The spectrometer was purged with dry nitrogen. Typically, 32 scans were recorded at a spectral resolution of 2 cm^{-1}. Either the spectrum of the pristine nanotubes or a commercial anatase reference (Hombikat UV-100) was used as background.

3 Results and Discussion

Figure 1 shows pristine protonated TiONTs at different magnifications. The as-synthesized elongated nanotubes are open-ended with a layered, rolled-up structure. In Fig. 1b the inner pore channel of these nanotubular materials is visible. The average TiONT length is 100–130 nm, the inner diameter is 5–6 nm and the outer diameter is 11–12 nm.

Previously we investigated the urea based ammonia doping of titanate nanotubes, similarly to those reported in [28, 35, 46]. During this process we observed that nanotubes completely morph into 25 nm long isotropic (cuboid and octahedral) nanoparticles. In Fig. 2. TEM images of pristine TiONT (a), and urea based NH_3 doped nanotubes (b) are compared. We successfully reproduced our previous results as demonstrated in Fig. 2b. NH_4F treatment also resulted
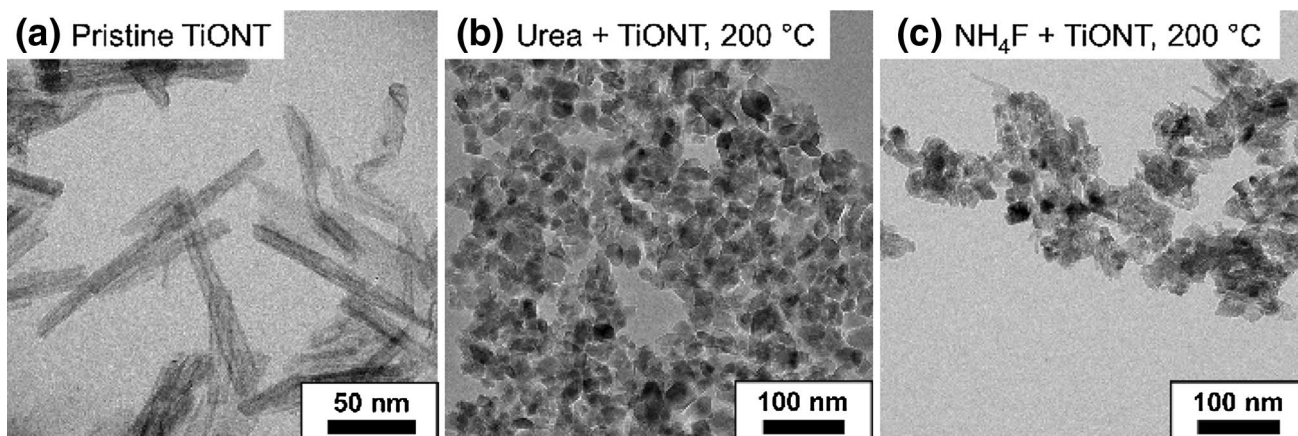

Fig. 1 TEM images of pristine protonated TiONTs in different magnifications (**a**, **b**). The inner pore channels of nanotubes are clearly seen in panel **b**

Fig. 2 TEM images of pristine titanate nanotubes (**a**) and after urea (**b**) and NH$_4$F (**c**) treatment at 200 °C

in the collapse of the nanotubes. It seems plausible that the acidic media enhanced TiONT degradation in this case [55].

As mentioned earlier, single crystal TiO$_2$ (scTiO$_2$) favors N embedding into its lattice upon N$_2^+$ ion bombardment [49]. XPS results corresponding to this ion implantation method are depicted in Fig. 3. The signal at 396.7 eV is characteristic for substitutional nitrogen bonded to metal. Peaks at 397.3 and 398.3 eV are due to N-containing ions in O–Ti–N bond on the surface (Fig. 3b). Reduced titania states are also formed during nitridation. Both Ti^{2+} and Ti^{3+} exist under these conditions [48]. This nitridation process took 20 min and the overall built-in nitrogen content was 16.1 at.%.

This experiment was repeated using TiONTs instead of scTiO$_2$. Interestingly, only 2.7 at.% nitrogen content was achieved by the similar 20 min long N$_2^+$ bombardment process. Figure 4a shows a doping-induced change in the Ti2p XP line shape. The small shoulder at around 456.0 eV is characteristic for the Ti^{3+} state. Figure 4b reveals N at B.E.

of 396.3 eV that is, in position substituting lattice oxygen [28, 35, 56–58], while other lines between 398 and 402 eV are characteristic for nitrogen trapped in different lattice defects surrounded by varying number of oxygens. Features at 398–400 eV are due to interstitial N [47], while photoemission peaks above 400 eV are typically attributed to either embedded N$_2$ or to nitrate/nitrite species [28].

Since the extent of nitrogen incorporation into TiONTs by N$_2^+$ bombardment is limited to low levels (approximately 3 at.%), the application of plasma treatment was considered. The first dopant source was N$_2$ plasma at 600 V bias voltage for 20 min. The positively charged N$_2^+$ plasma ions dissociate to two N atoms with an average energy of 300 eV each upon hitting the surface, thus the process is capable of building various types of nitrogen into the lattice. Figure 5a shows that essentially no reduced Ti states appear in this case, which also indicates that N incorporation in substitutional position is minimal. Indeed, only a weak N signal at B.E. 396 eV is observable (Fig. 5b) and N–O–Ti bonds are
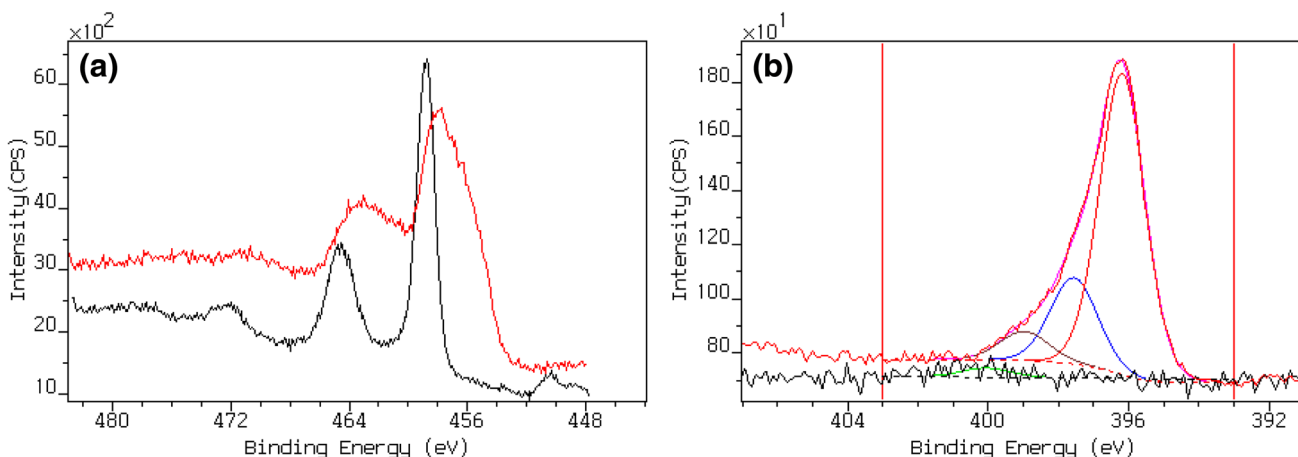

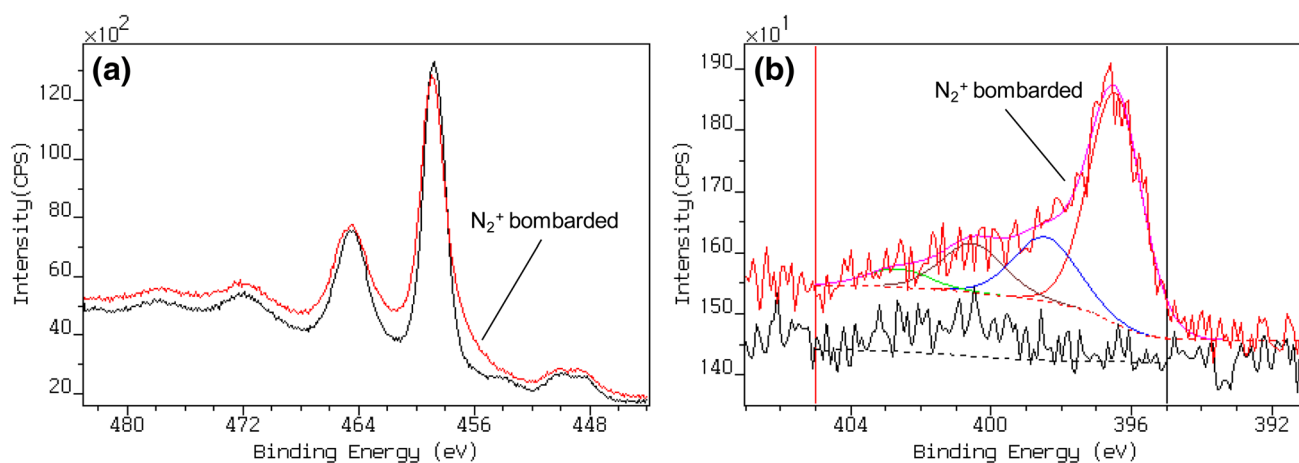**Fig. 3** XP lines of Ti2p (**a**) and N1s (**b**) of scTiO$_2$ before and after N$_2^+$ implantation process

Fig. 4 XP lines of Ti2p (**a**) and N1s (**b**) of TiONT before and after N_2^+ implantation
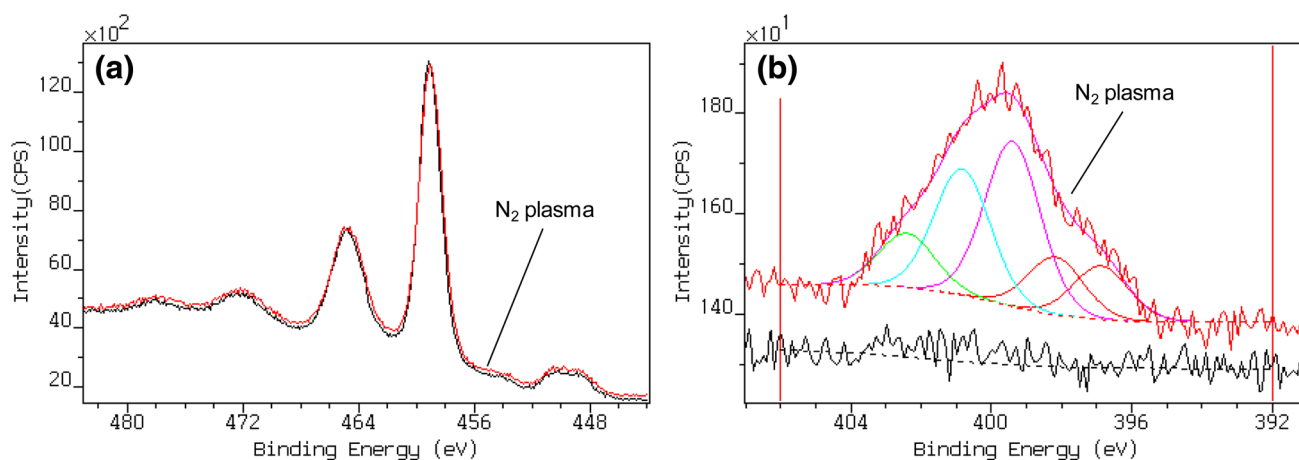

Fig. 5 XP lines of Ti2p (**a**) and N1s (**b**) of TiONT before and after N_2 plasma treatment process

formed besides other entrapped N species appearing in the 398–402 eV B.E. range. The explanation to the low degree of formation of Ti–N via ion bombardment and N_2 plasma treatment on TiONTs lies in the structure of the nanotubes. Unlike single crystal titania, titanates—even in their protonated forms—contain significant amounts of OH groups and structural water [5]. We suggest that this oxygen rich local surface environment hinders substitutional N incorporation in titanate nanotubes compared to single crystal TiO_2 [41].

To verify this hypothesis, TiONTs were treated in positively charged NH_3 plasma for 10 and 30 min at 300 V bias voltage. This bias condition ensured that the energy of N atoms actually interacting with the surface closely matched that relevant for N_2 plasma at 600 V bias. Figure 6a, b shows that indeed, more nitrogen is incorporated into the nanotubes from NH_3 plasma then from N_2 plasma. The achieved nitrogen content increased by one order of magnitude to 20.4 at.%. Three types of nitrogen are observable in the N1s region: the 396 eV photoemission belongs to the

substitutional (Ti–N) form, while the peaks at 398–399.5 and 400.5 eV can be attributed to different NH species [56, 59] and/or interstitial N [47]. The Ti2p XP lines also changed during the process: the Ti^{3+} peak developed at 456.0 eV indicating a successful, Ti–N bond forming N incorporation.

Figure 6c, d depict XP spectra of TiONTs N-doped by NH_3 generated *in situ* by urea decomposition. There are no significant differences in the Ti2p region between pristine and doped samples and one dominating type of N is observable in the N 1 s region at about 400 eV BE. This one is characteristic for N species built, most probably, into different defect sites surrounded by oxygen (400 eV B.E.). Such nitrogen bonding states were tentatively assigned to an N···H complex interstitially bound in the TiO_2 lattice [56, 57] and linked to the enhanced photocatalytic activity, even though the observed photo-threshold energy decrease was associated earlier exclusively with substitutional N at 396.5 eV B.E [35]. N doping was suggested to introduce localized N2p states within the band gap close to the top
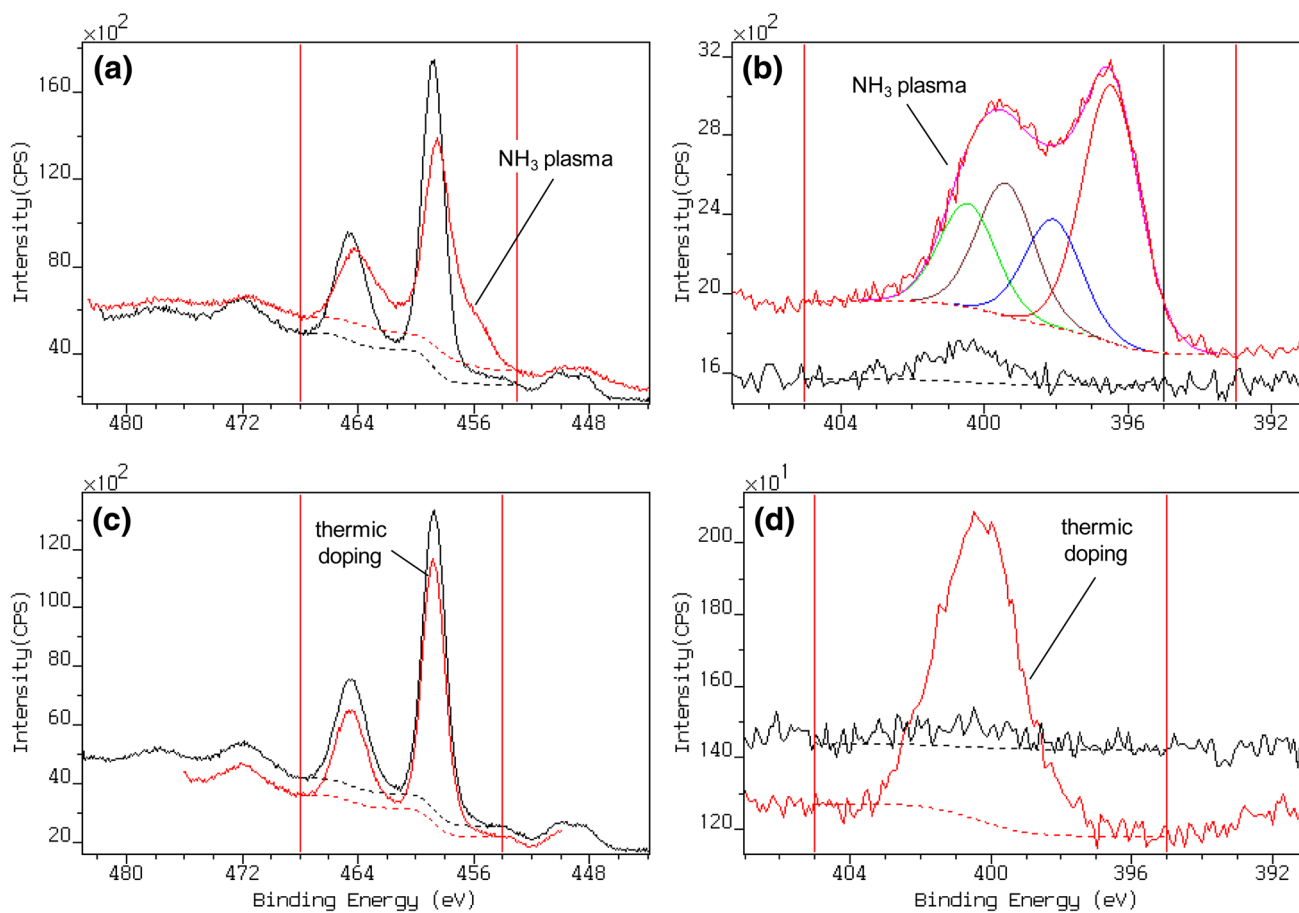
Fig. 6 XP lines of Ti2p and N1s of TiONT before and after NH_3 plasma nitridation (**a, b**) and urea based thermic doping (**c, d**) process

of the valence band, facilitating the production of oxygen vacancies and Ti3d states within the bandgap at elevated temperatures [60]. In the case of NH_4F treatment no photoemission at ~396 eV due to subtitutional N was detected. The Ti2p line remained unaltered.

Summarizing, XPS measurements depicted in Fig. 6. suggest that NH_3 plasma treatment is the most effective way to incorporate substitutional nitrogen into the lattice of TiONTs.

Fourier transform infrared spectroscopy (DRIFTS) was utilized to identify surface specimens formed during the doping process, i.e. to reveal the nature of the so-called "adsorbed nitrogen" species. Figure 7 depicts the DRIFTS spectra of TiONTs treated in NH_3 plasma for 30 min, as well as their urea-based and NH_4F thermally doped counterparts. IR bands were observed after NH_3 plasma treatment at around 3000, 1700–1560, 1434, and 1257 cm^{-1}. When urea was the precursor molecule, the same peaks with much higher intensities were detected between 3200–2800 cm^{-1} (3201, 3037, 2967, 2928, and 2854 cm^{-1}) and 1700–1200 cm^{-1} (1703, 1627, 1563, 1443, and 1257 cm^{-1}). A very similar IR spectrum was recorded

earlier on ammonium trititanate nanotubes (NH_4TNT) produced from sodium trititanate nanotubes by ion exchange using NH_4NO_3 [46]. The observed peaks were assigned to the N–H steching mode and the asymmetric bending mode of NH_4^+. Similar NH vibration features were observed after NH_3 adsorption on TiO_2 [61]. Bands at 1703, 1563 and 1257 cm^{-1} for NH_4 species were detected after adsorption of NH_4F on TNT (Fig. 7). Summarizing, the DRIFTS experiments confirmed the XPS results insofar as Ti–N formation is always accompanied by NH_4^+ group development in the studied processes [58]. It is important to emphasize that no bands indicative of nitrosyl species were detected in the 1950–1850 cm^{-1} range after NH_3 plasma treatment [62].
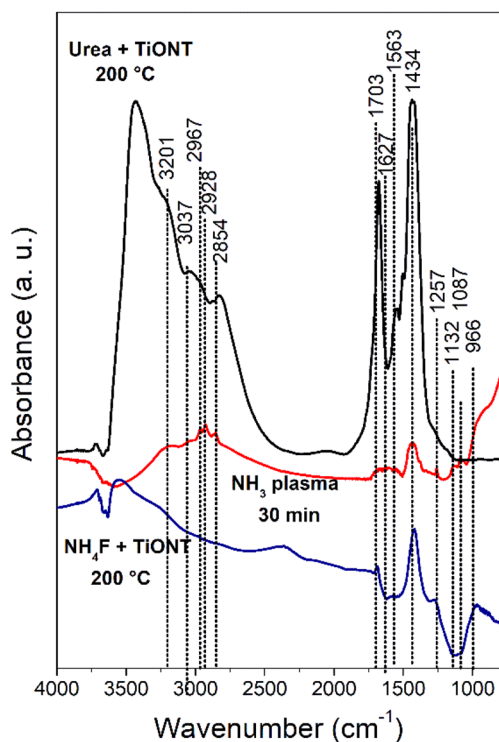
Fig. 7 DRIFT spectra of a NH_3 plasma treated sample and two thermally doped (urea and NH_4F decomposition) TiONT samples

Figure 8 depicts the morphology of pristine and N-doped titanate nanotubes on Al foil. It is remarkable that even though NH_3 plasma treatment was the best way to impose structural changes on TiONTs by incorporating nitrogen into the lattice, it left the tubular morphology intact. Indeed, SEM images in Fig. 8b, c. do not show any signs of nanotube morphing or collapse—the tubular structure was maintained during and after nitrogen incorporation.

The structure conserving nature of NH_3 plasma doping was confirmed by analyzing the crystallinity of the doped samples using XRD. Figure 9 depicts the XRD patterns of TiONT before and after the different nitridation processes.

The characteristic reflections are indicated in the figure. Characteristic reflections of TiONT ($2\theta = 9.66°$, $24.49°$, $28.08°$ and $48.5°$) match the literature data well [16]. The first broad reflection corresponds to the 0.74 nm interlayer distance between the rolled-up titanate sheet layers. It is clear that none of the plasma treatments affects the trititanate structure and there are no new phases in the system. In contrast, titanate reflections disappeared when either of the thermal doping processes was attempted, and new reflections with Miller indices of (101), (004), (200), (105), (211) and (204) appeared at $2\theta = 25.45°$, $37.06°$, $37.89°$, $38.74°$, $48.22°$, $53.97°$, and $55.17°$, respectively. This confirms that the trititanate structure recrystallized into anatase TiO_2 during the synthesis. However, the crystallinity degree of commercial anatase is higher than that of its thermal doping derived counterparts.

4 Conclusions

We presented a systematic study on N-doping in protonated titanate nanotubes utilizing N_2^+ bombardment, thermal and plasma based methods. NH_4^+ was detected on the surface in all cases. Single crystalline rutile TiO_2 bombarded with N_2^+ served as a doping benchmark. Methods based on the thermal decomposition of urea or NH_4F generate NH_3 *in situ*, but neither of them is capable of inserting substitutional nitrogen into the lattice. On the other hand, N_2^+ bombardment as well as N_2 and NH_3 plasma based methods can all yield N-doped nanotubes with the desired Ti–N bonds. This was clearly confirmed by monitoring the N XPS peak at around 396 eV, which is characteristic for nitrogen in this position and also by a low B.E. shoulder on the Ti2p line. The extent of nitridation depends on the type of the plasma and the duration of the treatment. Positively charged NH_3 plasma was found to be the most powerful way to incorporate nitrogen into the nanotube lattice in over 20 at.% loading. Surprisingly, this incorporation technique left both the
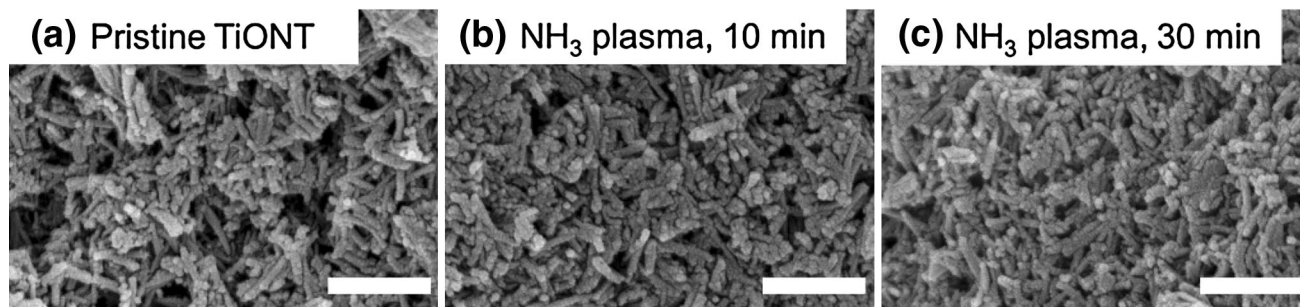

Fig. 8 FE-SEM images of pristine (**a**) and NH_3 plasma modified titanate nanotubes (**b–c**) on Al foil. The scale bar corresponds to 500 nm in all three images
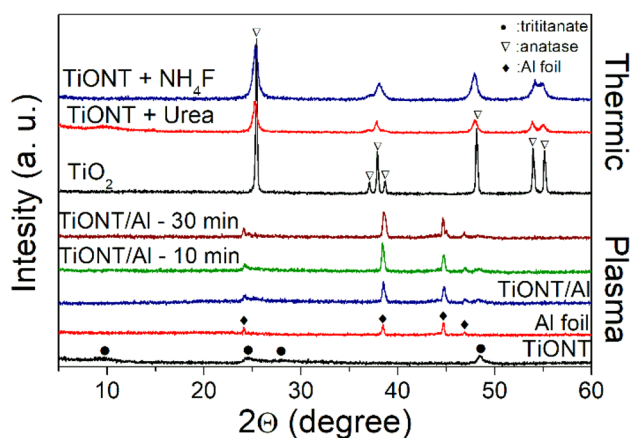
Fig. 9 XRD patterns of titanate nanotubes before and after different nitridation processes

tubular morphology and the titanate crystal structure of the nanotubes intact. Considering the high specific surface area of titanate nanotubes as well as the technological feasibility and scalability of the NH_3 plasma treatment, we believe that the reported results represent a step forward in the systematic design of highly efficient titanate based VLD photocatalysts.

References

1. Bavykin DV, Parmon VN, Lapkin AA, Walsh FC (2004) The effect of hydrothermal conditions on the mesoporous structure of TiO2 nanotubes. J Mater Chem 14(22):3370–3377. https://doi.org/10.1039/b406378c
2. Kasuga T, Hiramatsu M, Hoson A, Sekino T, Niihara K (1998) Formation of titanium oxide nanotube. Langmuir 14(12):3160–3163. https://doi.org/10.1021/la9713816
3. Pótári G, Madarász D, Nagy L, László B, Sápi A, Oszkó A, Kukovecz A, Erdohelyi A, Kónya Z, Kiss J (2013) Rh-induced support transformation phenomena in titanate nanowire and nanotube catalysts. Langmuir 29(9):3061–3072. https://doi.org/10.1021/la304470v
4. Kukovecz Á, Kordás K, Kiss J, Kónya Z (2016) Atomic scale characterization and surface chemistry of metal modified titanate nanotubes and nanowires. Surf Sci Rep 71(3):473–546. https://doi.org/10.1016/j.surfrep.2016.06.001
5. Buchholcz B, Haspel H, Boldizsár T, Kukovecz Á, Kónya Z (2017) pH-regulated antimony oxychloride nanoparticle formation on titanium oxide nanostructures: a photocatalytically active heterojunction. CrystEngComm 19(10):1408–1416. https://doi.org/10.1039/c6ce02340a
6. Buchholcz B, Haspel H, Oszkó A, Kukovecz A, Kónya Z (2017) Titania nanotube stabilized BiOCl nanoparticles in visible-light photocatalysis. RSC Adv 7(27):16410–16422. https://doi.org/10.1039/c6ra28490f
7. Sluban M, Cojocaru B, Parvulescu VI, Iskra J, Korošec RC, Umek P (2017) Protonated titanate nanotubes as solid acid catalyst for aldol condensation. J Catal 346:161–169. https://doi.org/10.1016/j.jcat.2016.12.015
8. Kuwahara Y, Fujie Y, Yamashita H (2017) Poly-(ethyleneimine)-tethered Ir complex catalyst immobilized in titanate nanotubes for hydrogenation of CO2 to formic acid. ChemCatChem 9(11):1906–1914. https://doi.org/10.1002/cctc.201700508
9. Aouadi I, Touati H, Tatibouët J-M, Bergaoui L (2017) Titanate nanotubes as ethanol decomposition catalysts: effect of coupling photocatalysis with non-thermal plasma. J Photochem Photobiol A 346:485–492. https://doi.org/10.1016/j.jphotochem.2017.06.030
10. Sandoval A, Hernández-Ventura C, Klimova TE (2017) Titanate nanotubes for removal of methylene blue dye by combined adsorption and photocatalysis. Fuel 198:22–30. https://doi.org/10.1016/j.fuel.2016.11.007
11. László B, Baán K, Varga E, Oszkó A, Erdőhelyi A, Kónya Z, Kiss J (2016) Photo-induced reactions in the CO2-methane system on titanate nanotubes modified with Au and Rh nanoparticles. Appl Catal B 199:473–484. https://doi.org/10.1016/j.apcatb.2016.06.057
12. Bavykin DV, Walsh FC (2007) Kinetics of alkali metal ion exchange into nanotubular and nanofibrous titanates. J Phys Chem C 111(40):14644–14651. https://doi.org/10.1021/jp073799a
13. Bavykin DV, Lapkin AA, Plucinski PK, Friedrich JM, Walsh FC (2005) Reversible storage of molecular hydrogen by sorption into multilayered TiO2 nanotubes. J Phys Chem B 109(41):19422–19427. https://doi.org/10.1021/jp0536394
14. Paris J, Bernhard Y, Boudon J, Heintz O, Millot N, Decréau R (2015) Phthalocyanine–titanate nanotubes: a promising nanocarrier detectable by optical imaging in the so-called imaging window. RSC Adv 5(9):6315–6322. https://doi.org/10.1039/c4ra13988g
15. Yang D, Wang X, Ai Q, Shi J, Jiang Z (2015) Performance comparison of immobilized enzyme on the titanate nanotube surfaces modified by poly-(dopamine) and poly-(norepinephrine). RSC Adv 5(53):42461–42467. https://doi.org/10.1039/c5ra02420j
16. Chen Q, Du G, Zhang S, Peng L-M (2002) The structure of trititanate nanotubes. Acta Crystallogr Sect B 58(4):587–593. https://doi.org/10.1107/S0108768102009084
17. Dmitry V, Walsh C (2010) Titanate and titania nanotubes: synthesis, properties and applications. Royal Society of Chemisty, Cambridge, https://doi.org/10.1039/9781849730778
18. Kukovecz Á, Hodos M, Horváth E, Radnóczi G, Kónya Z, Kiricsi I (2005) Oriented crystal growth model explains the formation of titania nanotubes. J Phys Chem B 109(38):17781–17783. https://doi.org/10.1021/jp054320m
19. Diebold U (2003) The surface science of titanium-dioxide. Surf Sci Rep 48(5):53–229. https://doi.org/10.1016/S0167-5729(02)00100-0
20. Wang L, Sasaki T (2014) Titanium-oxide nanosheets: graphene analogues with versatile functionalities. Chem Rev 114(19):9455–9486. https://doi.org/10.1021/cr400627u
21. Houas A, Lachheb H, Ksibi M, Elaloui E, Guillard C, Herrmann J-M (2001) Photocatalytic degradation pathway of methylene blue in water. Appl Catal B 31(2):145–157. https://doi.org/10.1016/S0926-3373(00)00276-9
22. Thiruvenkatachari R, Vigneswaran S, Moon IS (2008) A review on UV/TiO2 photocatalytic oxidation process (Journal Review). Korean J Chem Eng 25(1):64–72. https://doi.org/10.1007/s11814-008-0011-8
23. Halasi G, Schubert GB, Solymosi F (2012) Photodecomposition of formic acid on N-doped and metal-promoted TiO2 production

of CO-free H$_2$. J Phys Chem C 116(29):15396–15405. https://doi.org/10.1021/jp3030478

24. Kumar SG, Devi LG (2011) Review on modified TiO$_2$ photocatalysis under UV/visible light: selected results and related mechanisms on interfacial charge carrier transfer dynamics. J Phys Chem A 115(46):13211–13241. https://doi.org/10.1021/jp204364a

25. Rehman S, Ullah R, Butt A, Gohar N (2009) Strategies of making TiO$_2$ and ZnO visible light active. J Hazard Mater 170(2):560–569. https://doi.org/10.1016/j.jhazmat.2009.05.064

26. Qin W, Zhang D, Zhao D, Wang L, Zheng K (2010) Near-infrared photocatalysis based on YF$_3$: Yb^{3+}, Tm^{3+}/TiO$_2$ core/shell nanoparticles. Chem Commun 46(13):2304–2306. https://doi.org/10.1039/b924052g

27. Tang Y, Di W, Zhai X, Yang R, Qin W (2013) NIR-responsive photocatalytic activity and mechanism of NaYF$_4$: Yb, Tm@ TiO$_2$ core–shell nanoparticles. ACS Catal 3(3):405–412. https://doi.org/10.1021/cs300808r

28. Henderson MA (2011) A surface science perspective on photocatalysis. Surf Sci Rep 66(6):185–297. https://doi.org/10.1016/j.surfrep.2011.01.001

29. Park MS, Kwon S, Min B (2002) Electronic structures of doped anatase TiO$_2$: Ti$_{1-x}$M$_x$O$_2$ (M = Co, Mn, Fe, Ni). Phys Rev B 65(16):161201. https://doi.org/10.1103/PhysRevB.65.161201

30. Kočí K, Matějů K, Obalová L, Krejčíková S, Lacný Z, Plachá D, Čapek L, Hospodková A, Šolcová O (2010) Effect of silver doping on the TiO$_2$ for photocatalytic reduction of CO$_2$. Appl Catal B 96(3):239–244. https://doi.org/10.1016/j.apcatb.2010.02.030

31. Dozzi MV, Selli E (2013) Doping TiO$_2$ with p-block elements: effects on photocatalytic activity. J Photochem Photobiol C 14:13–28. https://doi.org/10.1016/j.jphotochemrev.2012.09.002

32. Devi LG, Kavitha R (2013) A review on non metal ion doped titania for the photocatalytic degradation of organic pollutants under UV/solar light: role of photogenerated charge carrier dynamics in enhancing the activity. Appl Catal B 140:559–587. https://doi.org/10.1016/j.apcatb.2013.04.035

33. Serpone N (2006) Is the band gap of pristine TiO$_2$ narrowed by anion- and cation-doping of titanium dioxide in second-generation photocatalysts? J Phys Chem B 110(48):24287–24293. https://doi.org/10.1021/jp065659r

34. Gracia F, Holgado JP, Caballero A, Gonzalez-Elipe AR (2004) Structural, optical, and photoelectrochemical properties of M^{n+}–TiO$_2$ model thin film photocatalysts. J Phys Chem B 108(45):17466–17476. https://doi.org/10.1021/jp0484938

35. Asahi R, Morikawa T, Ohwaki T, Aoki K, Taga Y (2001) Visible-light photocatalysis in nitrogen-doped titanium oxides. Science 293(5528):269–271. https://doi.org/10.1126/science.1061051

36. Sato S (1986) Photocatalytic activity of NO$_x$-doped TiO$_2$ in the visible light region. Chem Phys Lett 123(1–2):126–128. https://doi.org/10.1016/0009-2614(86)87026-9

37. Jagadale TC, Takale SP, Sonawane RS, Joshi HM, Patil SI, Kale BB, Ogale SB (2008) N-doped TiO$_2$ nanoparticle based visible light photocatalyst by modified peroxide sol–gel method. J Phys Chem C 112(37):14595–14602. https://doi.org/10.1021/jp803567f

38. Hanaor DA, Sorrell CC (2011) Review of the anatase to rutile phase transformation. J Mater Sci 46(4):855–874. https://doi.org/10.1007/s10853-010-5113-0

39. Buchholcz B, Varga E, Varga T, Plank K, Kiss J, Kónya Z (2017) Structure and stability of boron doped titanate nanotubes and nanowires. Vacuum 138:120–124. https://doi.org/10.1016/j.vacuum.2016.11.038

40. Pusztai P, Puskás R, Varga E, Erdőhelyi A, Kukovecz Á, Kónya Z, Kiss J (2014) Influence of gold additives on the stability and phase transformation of titanate nanostructures. Phys Chem Chem Phys 16(48):26786–26797. https://doi.org/10.1039/c4cp04084h

41. Halasi G, Schubert G, Solymosi F (2012) Comparative study on the photocatalytic decomposition of methanol on TiO$_2$ modified by N and promoted by metals. J Catal 294:199–206. https://doi.org/10.1016/j.jcat.2012.07.020

42. Joung S-K, Amemiya T, Murabayashi M, Itoh K (2006) Relation between photocatalytic activity and preparation conditions for nitrogen-doped visible light-driven TiO$_2$ photocatalysts. Appl Catal A 312:20–26. https://doi.org/10.1016/j.apcata.2006.06.027

43. Wang Z, Cai W, Hong X, Zhao X, Xu F, Cai C (2005) Photocatalytic degradation of phenol in aqueous nitrogen-doped TiO$_2$ suspensions with various light sources. Appl Catal B 57(3):223–231. https://doi.org/10.1016/j.apcatb.2004.11.008

44. Di Valentin C, Finazzi E, Pacchioni G, Selloni A, Livraghi S, Paganini MC, Giamello E (2007) N-doped TiO$_2$: theory and experiment. Chem Phys 339(1):44–56. https://doi.org/10.1016/j.chemphys.2007.07.020

45. Buchholcz B, Haspel H, Kukovecz Á, Kónya Z (2014) Low-temperature conversion of titanate nanotubes into nitrogen-doped TiO$_2$ nanoparticles. CrystEngComm 16(32):7486–7492. https://doi.org/10.1039/c4ce00801d

46. Chang J-C, Tsai W-J, Chiu T-C, Liu C-W, Chao J-H, Lin C-H (2011) Chemistry in a confined space: characterization of nitrogen-doped titanium oxide nanotubes produced by calcining ammonium tri-titanate nanotubes. J Mater Chem 21(12):4605–4614. https://doi.org/10.1039/c0jm03058a

47. Maeda M, Watanabe T (2006) Visible light photocatalysis of nitrogen-doped titanium oxide films prepared by plasma-enhanced chemical vapor deposition. J Electrochem Soc 153(3):C186-C189. https://doi.org/10.1149/1.2165773

48. Bertóti I (2012) Nitrogen modified metal oxide surfaces. Catal Today 181(1):95–101. https://doi.org/10.1016/j.cattod.2011.06.017

49. Sullivan JL, Saied SO, Bertoti I (1991) Effect of ion and neutral sputtering on single crystal TiO2. Vacuum 42(18):1203–1208. https://doi.org/10.1016/0042-207X(91)90131-2

50. Bertóti I, Kelly R, Mohai M, Tóth A (1992) A possible solution to the problem of compositional change with ion-bombarded oxides. Surf Interface Anal 19(1–12):291–297. https://doi.org/10.1002/sia.740190155

51. Bertóti I, Kelly R, Mohai M, Tóth A (1993) Response of oxides to ion bombardment: the difference between inert and reactive ions. Nuclear Instrum Methods Phys Res Sect B 80–81 (Part 2):1219–1225. https://doi.org/10.1016/0168-583X(93)90770-7

52. Mohai M (2004) XPS MultiQuant: multimodel XPS quantification software. Surf Interface Anal 36(8):828–832. https://doi.org/10.1002/sia.1775

53. Mohai M, Bertoti I (2004) Calculation of overlayer thickness on curved surfaces based on XPS intensities. Surf Interface Anal 36(8):805–808. https://doi.org/10.1002/sia.1769

54. Reilman RF, Msezane A, Manson ST (1976) Relative intensities in photoelectron spectroscopy of atoms and molecules. J Electron Spectrosc Relat Phenom 8(5):389–394. https://doi.org/10.1016/0368-2048(76)80025-4

55. Bavykin DV, Friedrich JM, Lapkin AA, Walsh FC (2006) Stability of aqueous suspensions of titanate nanotubes. Chem Mater 18(5):1124–1129. https://doi.org/10.1021/cm0521875

56. Diwald O, Thompson TL, Zubkov T, Walck SD, Yates JT (2004) Photochemical activity of nitrogen-doped rutile TiO$_2$(110) in visible light. J Phys Chem B 108(19):6004–6008. https://doi.org/10.1021/jp031267y

57. Thompson TL, Yates JT (2006) Surface science studies of the photoactivation of TiO$_2$—new photochemical processes. Chem Rev 106(10):4428–4453. https://doi.org/10.1021/cr050172k

58. Beranek R, Kisch H (2008) Tuning the optical and photoelectrochemical properties of surface-modified TiO$_2$. Photochem Photobiol Sci 7(1):40–48. https://doi.org/10.1039/B711658F

59. Souto S, Alvarez F (1997) The role of hydrogen in nitrogen-containing diamondlike films studied by photoelectron spectroscopy. Appl Phys Lett 70(12):1539–1541. https://doi.org/10.1063/1.118611

60. Batzill M, Morales EH, Diebold U (2006) Influence of nitrogen doping on the defect formation and surface properties of TiO_2 rutile and anatase. Phys Rev Lett 96(2):026103. https://doi.org/10.1103/PhysRevLett.96.026103

61. Jung SM, Grange P (2000) The investigation of mechanism of SCR reaction on a TiO_2-SO_4^{2-} catalyst by DRIFTS. Appl Catal B 27(1):L11-L16. https://doi.org/10.1016/S0926-3373(00)00145-4

62. Ramis G, Busca G, Lorenzelli V, Forzatti P (1990) Fourier transform infrared study of the adsorption and coadsorption of nitric oxide, nitrogen dioxide and ammonia on TiO_2 anatase. Appl Catal 64:243–257. https://doi.org/10.1016/S0166-9834(00)81564-X